



ELSEVIER

Contents lists available at SciVerse ScienceDirect

Developmental Biology

journal homepage: www.elsevier.com/locate/developmentalbiology

*Ndr*2 regulates vertebral specification in differentiating somites

Huang Zhu^a, Jianzhi Zhao^a, Wenrong Zhou^a, Hanjun Li^a, Rujiang Zhou^a, Lingling Zhang^a, Haixia Zhao^a, Jingjing Cao^a, Xuming Zhu^a, Hongliang Hu^c, Gang Ma^a, Lin He^a, Zhengju Yao^a, Libo Yao^b, Xizhi Guo^{1,a,*}

^a Bio-X Institutes, Key Laboratory for the Genetics of Developmental and Neuropsychiatric Disorders (Ministry of Education), Shanghai Jiao Tong University, Shanghai 200240, China

^b Department of Biochemistry and Molecular Biology, State Key Laboratory of Cancer Biology, The Fourth Military Medical University, Xi'an 710032, China

^c Renji Hospital, Shanghai Jiao Tong University, Shanghai 200240, China

ARTICLE INFO

Article history:

Received 17 April 2012

Received in revised form

29 June 2012

Accepted 2 July 2012

Available online 20 July 2012

Keywords:

*Ndr*2

Vertebral patterning

Differentiating somites

Homeotic transformation

Hox genes

Bmp/Smad signaling

ABSTRACT

It is generally thought that vertebral patterning and identity are globally determined prior to somite formation. Relatively little is known about the regulators of vertebral specification after somite segmentation. Here, we demonstrated that *Ndr*2, a tumor suppressor gene, was dynamically expressed in the presomitic mesoderm (PSM) and at early stage of differentiating somites. Loss of *Ndr*2 in mice resulted in vertebral homeotic transformations in thoracic/lumbar and lumbar/sacral transitional regions in a dose-dependent manner. Interestingly, the inactivation of *Ndr*2 in osteoblasts or chondrocytes caused defects resembling those observed in *Ndr*2^{-/-} mice, with a lower penetrance. In addition, forced overexpression of *Ndr*2 in osteoblasts or chondrocytes also conferred vertebral defects, which were distinct from those in *Ndr*2^{-/-} mice. These genetic analyses revealed that *Ndr*2 modulates vertebral identity in segmented somites rather than in the PSM. At the molecular level, combinatory alterations of the amount of *Hoxc8-11* gene transcripts were detected in the differentiating somites of *Ndr*2^{-/-} embryos, which may partially account for the vertebral defects in *Ndr*2 mutants. Nevertheless, Bmp/Smad signaling activity was elevated in the differentiating somites of *Ndr*2^{-/-} embryos. Collectively, our findings unveiled *Ndr*2 as a novel regulator of vertebral specification in differentiating somites.

© 2012 Elsevier Inc. All rights reserved.

Introduction

The mammalian axial skeleton consist of cervical, thoracic, lumbar, sacral and caudal vertebrae, which exhibit regionalized morphological characteristics in the anterior–posterior (AP) direction (Burke et al., 1995). Vertebral development can be divided into two phases: the early stage of somite segmentation from the presomitic mesoderm (PSM) and the later stage of somitic patterning and specification (Hirsinger et al., 2000). A widely accepted model of somitogenesis is clock and wavefront model in which a temporal periodicity in presomitic mesoderm (PSM) coupled with a morphogen gradient (Such as *Fgf*, *Wnt*) to guide the periodic somite formation (Dequeant and Pourquie, 2008; Dubrulle and Pourquie, 2004; Pourquie, 2011). Somitic patterning and differentiation specifies vertebral morphology and identity, including the migration and osteochondrogenic differentiation of

the sclerotomal mesoderm in each segmented somite (Hirsinger et al., 2000).

The vertebral patterning and identity along the AP axis of the embryo is generally considered to be globally determined prior to somite formation (Alexander et al., 2009; Carapuco et al., 2005; Juan and Ruddle, 2003; Kieny et al., 1972; Nowicki and Burke, 2000). Once the somite buds off from the PSM, it will acquire its identity and morphological characteristics according to the pre-endowed patterning instructions from the PSM. In inactivating *Wnt3a*, *Notch*, *Fgf* or *RA* signaling mutants, homeotic transformations in different regions are observed in the axial skeletons; these transformations are usually correlated with alterations in the expression patterns of the *Hox* genes (Alexander et al., 2009; Aulehla et al., 2003; Dubrulle et al., 2001; Ikeya and Takada, 2001; Kessel and Gruss, 1991; Partanen et al., 1998). In addition, some mutations of the Bmp signaling pathway also affect vertebral patterning and identity (Ikeya et al., 2006; Katagiri et al., 1998; McMahon et al., 1998; McPherron et al., 1999; Miura et al., 2006; Oh and Li, 1997). In particular, mutations of *Gdf11* or *ActRIIB* lead to homeotic transformations throughout the axial skeleton (Lee et al., 2010; McPherron et al., 1999; Oh and Li, 1997; Oh et al., 2002).

* Corresponding author. Fax: 86 21 34206736.

E-mail address: xzguo2005@sjtu.edu.cn (X. Guo).

¹ Present address: #800 Dongchuan Road, Biomedical Building #1–205, Shanghai 200240, China.

Hox gene expression patterns are believed to form a “*Hox* code” essential for normal vertebral patterning (Alexander et al., 2009; Iimura et al., 2009; Iimura and Pourquie, 2007; Krumlauf, 1994; Mallo et al., 2010; Tschopp and Duboule, 2011; Wellik, 2007; Young and Deschamps, 2009). In mice, 39 *Hox* genes are organized into four collinear clusters on chromosomes and can be subdivided into 13 paralogous groups based on their similarities in both sequence and position (Alexander et al., 2009; Maconochie et al., 1996). *Hox* gene expression along the vertebrate AP axis exhibits a collinear pattern in which the expression boundary of a given *Hox* gene is usually related to its chromosomal position (Kmita and Duboule, 2003; Tschopp and Duboule, 2011). The temporal collinearity of the *Hox* genes is translated into a spatial collinear expression along the AP axis, defining the region-specific identity of vertebrae. The loss-of-function and gain-of-function mutants of *Hox* genes usually display vertebral homeotic transformations (Alexander et al., 2009; Wellik, 2007, 2009).

Ndr2 (N-Myc downstream regulated gene 2) was first identified as one of the *Ndr* family members (*Ndr1–4*) (Okuda and Kondoh, 1999). The *Ndr* family is highly conserved in phylogeny, as human *NDR2* exhibits 95% amino acid sequence identity with the mouse homolog. Human *Ndr* family members also share 53%–65% amino acid sequence identity with each other (Hwang et al., 2011; Yao et al., 2008). Recently, crystal structural analysis suggests that *Ndr2* is a non-enzymatic member of the α/β hydrolase superfamily because it lacks some important residues and has an occluded substrate binding site (Hwang et al., 2011). Despite these observations, the molecular and cellular functions of *Ndr2*, a cytoplasmic protein, are still unclear (Li et al., 2011). During mouse embryonic development, *Ndr2* is mainly detected in the brain, heart, liver, kidney, skeletal muscle, limb bud and somites (Hu et al., 2006; Okuda and Kondoh, 1999) and is involved in the development of multiple organs (Dupays et al., 2009; Foletta et al., 2009; Takahashi et al., 2005; Yang et al., 2010). Furthermore, the accumulated data also suggest that *Ndr2* is a potential tumor suppressor gene (Yao et al., 2008). However, the role of *Ndr2* during mouse embryogenesis is still poorly understood due to the lack of *Ndr2* loss-of-function analyses based on mouse genetics.

In this study, we generated *Ndr2* gain-of-function and loss-of-function mutant mice. Analyses of the vertebral defects in these mutants suggest that *Ndr2* is a novel regulator of vertebral patterning and morphogenesis in differentiating somites rather than in the PSM. *Ndr2* may exert its effect on vertebral specification, partially through regulating the expression of *Hox* genes and inhibiting Bmp/Smad signaling activity.

Materials and methods

Mice

Ndr2^{c/c} mutant mice were generated by Organism Biodel, China. An *Ndr2* genomic clone was isolated from BAC libraries (bMQ-181G14). Targeted 129S_v/E_v ES cells were identified by PCR using P1: 5'AGATTGAGTGTGAACGCTAAATAATG plus P2: 5'AGG-TGCCACTCCCCTGTCCTTCCTA and P3: 5'CTGAGCCCAGAAAG-CGAAGGA plus P4: 5'GGTAACTTCTCCACAAAGGTTAAGAG, producing 4424 and 4824 bp products, respectively. The floxed allele was identified by PCR using P5: 5'AAAAGCTCTCGTGTGTTCTGGCGT, P6: 5'CAGGAGAGGATGAAGGTTAGTGTAG, and P7: 5'ATCAGGATGATCTGGACGAAGAG, which produce 577 and 844 bp products from the wild type and floxed alleles, respectively. Mice carrying the *Ndr2* floxed allele were crossed with *Actin-Cre* (Jackson Laboratories, Bar Harbor, ME) transgenic mice

to obtain null allele. Male offspring with *Actin-Cre* allele were further mated to wild type C57BL/6 female mice to generate conventional null heterozygotes (*Ndr2*[±], without *Actin-Cre* allele). Then *Ndr2*[±] mice were crossed to each other to generate *Ndr2*^{-/-} mice. The null allele was identified by PCR using P5 and P8: 5'GTCATTGGGAGAATGGAGGAGGCA, which amplified a 724 bp fragment. Osteoblast-specific and chondrocyte-specific *Ndr2* conditional knockout mice were generated by crossing female *Ndr2*^{c/c} homozygous mice with *Col1a1-Cre* (3.6 kb) (Liu et al., 2004; Zha et al., 2008) and *Col2a1-Cre* (Ovchinnikov et al., 2000) males, respectively. Then, *Col1a1-Cre; Ndr2*^{c/+} or *Col2a1-Cre; Ndr2*^{c/+} males were backcrossed to female *Ndr2*^{c/c} mice.

Col1a1 (3.6 kb)-*Ndr2* and *Col2a1-Ndr2* transgenic mice were generated by our lab using the FVB/NJ or ICR/CD1 mouse strains. The *Ndr2* cDNA clone was obtained from ATCC clones (BC012963 ATCC, USA). The *Col1a1* (3.6 kb) promoter and *Col2a1* promoter were the same as those used in generating the transgenic *Cre* mice. The genotyping primers for the *Col1a1-Ndr2* and *Col2a1-Ndr2* mice were as follows: *Col1a1-Ndr2* forward: 5'CACTCCA-GTGACAGCACCTCT, reverse: 5'GGCTCCAACCAACTCCAATT; *Col2a1-Ndr2* forward: 5'GAAACAACCTACACCCTGG.

TCATCA, reverse: 5'CCGACGAAGTTCTGTATGATCTC. To analyze the activity of Wnt/ β -catenin signaling, *Ndr2* null mice were crossed with *BatGal* mice (Jackson Laboratories, Bar Harbor, ME), and β -gal staining was performed using X-gal as substrate.

RNA in situ hybridization and immunostaining

RNA in situ hybridization was performed as previously described (Guo et al., 2004) using digoxin-labeled probes for *Bmp4*, *Fgf8*, *Hoxd13* (Liu et al., 2012), *Lef1* (Guo et al., 2004), *Wnt3a*, and *EN-1* (kindly provided by Dr. A.L. Joyner). The following probes were synthesized using their complete cDNA clones as templates: *Ndr2* (BC012963), *Hoxa9* (BC055059), *Hoxc9* (BC050838), *Hoxa10* (BC050839), *Hoxc10* (BC053405) and *Hoxd10* (BC048690). Constructs for the rest of probes used in this study were prepared in our lab, and the primers for these constructs are listed in Supplementary Table S1.

For immunostaining, embryos were fixed in 4% paraformaldehyde and incubated in 30% sucrose and were then sectioned at 10 μ m. Primary antibodies against *Ndr2* (sc-50345, Santa Cruz, USA) and *MyoD* (554130, BD Biosciences, USA) and secondary antibodies conjugated to Alexa Fluor[®]488 and Alexa Fluor[®]594 (Invitrogen, CA, USA) were used in immunostaining. Antibody-labeled sections were counterstained with DAPI fluorescent dye (Southern Biotech, AB, USA) and observed and photographed using a Leica SP5 (Leica, German) confocal microscope.

Semi-quantitative and quantitative RT-PCR and Western blot

Total RNA from cultured cells or tissues was isolated using Trizol reagent (Invitrogen, CA, USA). cDNA was then synthesized using the SuperScript[™] III First-Strand Synthesis System (Invitrogen, CA, USA). For semi-quantitative RT-PCR, 1 μ g of cDNA was subjected to PCR analysis using the primers listed in Supplementary Table S1. The quantitative RT-PCRs were performed on an Applied Biosystems 7500 using SYBR reagents (04913850001, Roche, Switzerland). Primer sequences are also provided in Supplementary Table S1.

Proteins derived from somites of 12–25 of embryos at E11.5 and cell lysates were subjected to western blot analysis using standard technologies. Embryo trunks and cultured cells were lysed in T PER[®] tissue protein extraction reagent (78510, Thermal Scientific) and NP40 lysis buffer, respectively. The western blots were probed with the primary antibodies anti-*Ndr2* (sc-100787, Santa Cruz, USA), anti-Smad1 (9743, Cell Signaling, USA),

anti-phosphorylated-Smad1/5/8 (9511, Cell signaling, USA), or anti- β -actin (sc-69879, Santa Cruz, USA), followed by treatment with HRP-conjugated secondary antibodies. Positive signals were visualized using a Pierce ECL western blotting substrate detection Kit (32132, Pierce, USA). For quantification, the images were analyzed and quantitated in Adobe Photoshop following the method outlined at <http://www.lukemiller.org/journal/2007/08/quantifying-western-blot-without.html>.

Skeletal analysis

Skeletal analysis of newborn mice and 1-month-old mice were performed using the Alcian Blue/Alizarin Red S staining methods as previously described (Zhu et al., 2012).

Cell culture and transfection

The ATDC5 mouse chondrogenic cells were cultured in a 1:1 mixture of Dulbecco's modified Eagle's medium and Ham's F-12 medium (DMEM/F12, GIBCO) containing 5% fetal bovine serum (FBS, GIBCO). Cell lines were stably transfected with pCDNA-*Ndr2* or pCDNA-GFP using the MSCV retrovirus Retroviral Expression System (634401, Clontech) according to the manufacturer's instructions. Viruses were harvested and used for the transduction of ATDC5.

Results

Ndr2 is expressed in the presomitic mesoderm and differentiating somites

To characterize *Ndr2* expression during somitogenesis, we performed in situ hybridization (ISH) and immunostaining. At E8.5 and E9.5, *Ndr2* was faintly expressed in the PSM (Fig. 1A and C), which was labeled using *Fgf8* (Fig. 1B and D). By the time neural tube closure was completed, cells of the paraxial mesoderm were generated by tail bud (Cambray and Wilson, 2007). *Ndr2* was continuously expressed in tail bud (black arrows in Fig. 1E, G and H'). In the differentiating somites, *Ndr2* exhibited a dynamic expression pattern. At E9.5, *Ndr2* was markedly expressed in the anterior somites S1–S7 (red arrows

in Fig. 1C). After E10.5, *Ndr2* expression was restricted to the posterior somites and decreased anteriorly (Fig. 1E–H'). Through ISH and IHC examination on sections of E10.5 embryos, *Ndr2* expression was extensively detected in the majority of sclerotome and the surrounding mesoderm, including the somitic mesoderm layer and splanchnic mesoderm layer (Fig. 1I–J'). However, *Ndr2* expression was remarkably decreased at later stage of chondrogenic differentiation of sclerotome mesoderm (Data not shown). These results indicate that *Ndr2* was preferentially expressed at the early stage of somite differentiation. In addition, *Ndr2* was strongly expressed in the developing heart as reported previously (Fig. 1C, E and G), as well as in the limb buds and forebrain at E12.5 (Fig. 1H). The dynamic expression of *Ndr2* in the PSM and differentiating somites indicates a potential role of *Ndr2* in axial specification.

Generation of *Ndr2* knockout mice

To reveal the role of *Ndr2* in vertebral morphogenesis, we generated a mouse line carrying the *Ndr2* conditional knockout allele (*Ndr2*^{cl/c}) with exon2–6 flanked by LoxP sites (Fig. 2A and B). Female homozygotes (*Ndr2*^{cl/c}) were crossed to *Actin-Cre* transgenic male mice, which have ubiquitous *Cre* activity. Male offspring with *Actin-Cre* allele were further mated to wild type C57BL/6 female mice to generate conventional null allele (*Ndr2*[±]). The conditional and null alleles were identified by PCR (Fig. 2C). To assess the depletion efficiency, RNA and protein extracted from wild type, *Ndr2*[±] and *Ndr2*^{-/-} newborn mice or embryos were subjected to RT-PCR and western blotting, respectively (Fig. 2D and E). All these results demonstrate that *Ndr2* mRNA and protein expression are completely depleted in the knockout mice.

Loss of *Ndr2* modulates the vertebral identity in a dose-dependent manner

The homozygous *Ndr2* knockout mice (*Ndr2*^{-/-}) were viable and fertile with no apparent growth defects. However, *Ndr2*-deficient mice exhibited several homeotic transformations in the axial skeleton (Figs. 3 and 4 and Table 1). In wild type C57BL/6 mice, the axial skeleton usually consists of 7 cervical vertebrae, 13

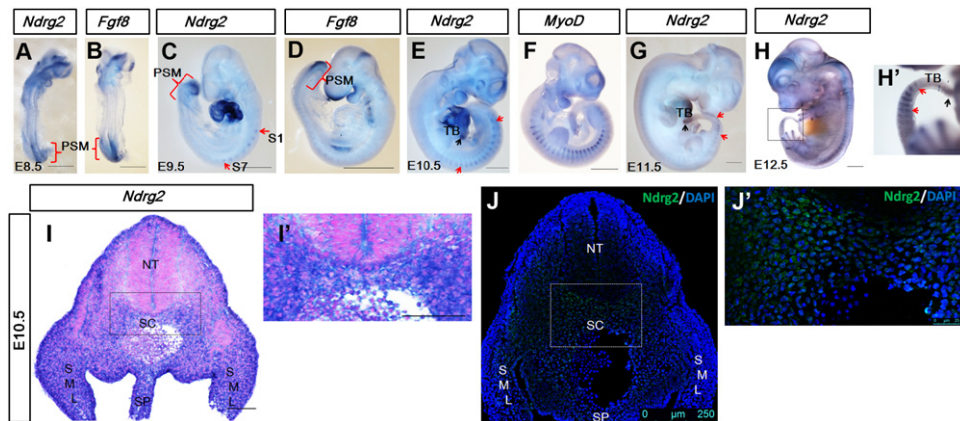


Fig. 1. Expression pattern of *Ndr2* during somite patterning and differentiation. The expression of *Ndr2* during somitogenesis was examined by in situ hybridization and immunostaining. (A–D) *Ndr2* is weakly expressed in the PSM at E8.5 (A) and in anterior somites (S1–S7) at E9.5 (C). The PSM is marked by *Fgf8* (B, D). (E–H') *Ndr2* expression is mainly detected in the posterior somites and decreases anteriorly at E10.5 (E), E11.5 (G) and E12.5 (H, H'). Somites at E10.5 are visualized by ISH for *MyoD* (F). *Ndr2* is continually expressed in the distal tip of tail bud (black arrows in E, G and H'). The red arrows mark the boundary of *Ndr2* expression. At E12.5, *Ndr2* is also observed in the developing limb buds and forebrain (H). (I, I') ISH for *Ndr2* in frozen section of somites at E10.5, showing that *Ndr2* is extensively expressed in the sclerotome mesoderm and surrounding mesoderm, including SML and SP. (I') Power view of rectangular area shown in (I). (J, J') Immunostaining for *Ndr2* on frozen sections of somites at E10.5. *Ndr2* is similarly detected in the extensive mesoderm including SC, SML and SP. Nuclei are stained with DAPI. The rectangle in (J) indicates the area shown at a higher magnification in (J'). PSM, presomitic mesoderm; TB, tail bud; NT, neural tube; SML, somitic mesoderm layer; SP, splanchnic mesoderm layer. Scale bars: in A–B, 500 μ m; in C–H', 1 mm; in I and I', 100 μ m; in J, 250 μ m; in J', 25 μ m.

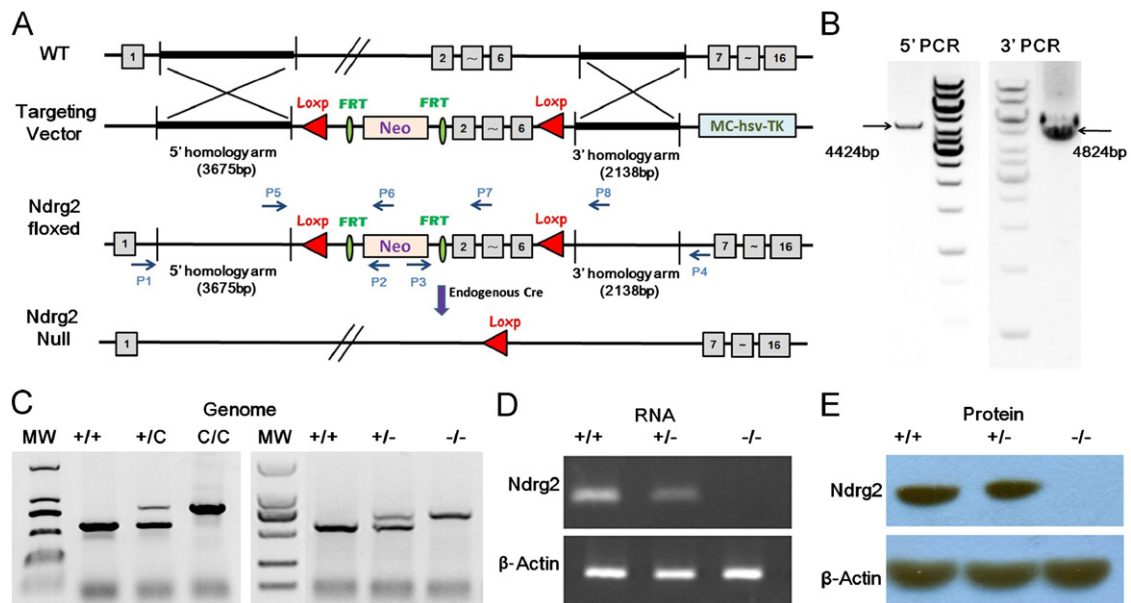


Fig. 2. Conditional targeted strategy for *Ndrgr2* locus. (A) Schematic representation of the *Ndrgr2* wild-type locus (wild type, top), targeting vector (middle), targeted allele (*Ndrgr2*-floxed, middle), and null allele (*Ndrgr2*-Null, bottom). Exons are represented by solid rectangles. The targeting vector, which is flanked by 3675 bp of 5' homology and 2138 bp of 3' homology, contains a LoxP-Frt-Neo-Frt cassette and the second LoxP sequence in introns 1 and 6, respectively. (B) Genomic PCR for the recombinant ES cell line. The recombinant is isolated by oligos P1/P2 for the 5' arm and P3/P4 for the 3' arm (marked in A), generating 4424 and 4484 bp PCR fragments, respectively. Oligos (P1–P4) positions are indicated below the *Ndrgr2*-floxed allele. (C) PCR genotyping of *Ndrgr2* mutant mice. Four oligos (P5–P8) for the PCR of *Ndrgr2* alleles are also marked by arrows in (A). P5/P7 amplifies a 577 bp fragment for the wild-type allele (+), P5/P6 generates a 826 bp fragment for the floxed allele (c), whereas P5/P8 produces a 724 bp fragment for the null allele (–). (D) RT-PCR analysis of *Ndrgr2* expression in wild-type, heterozygous and null mice at P0. Total RNA is extracted from the liver. (E) Western blotting analysis of *Ndrgr2* protein in wild-type, heterozygous and null embryos at E11.5. Protein was extracted from cells of the 12th somite (S12) to the 25th somite (S25).

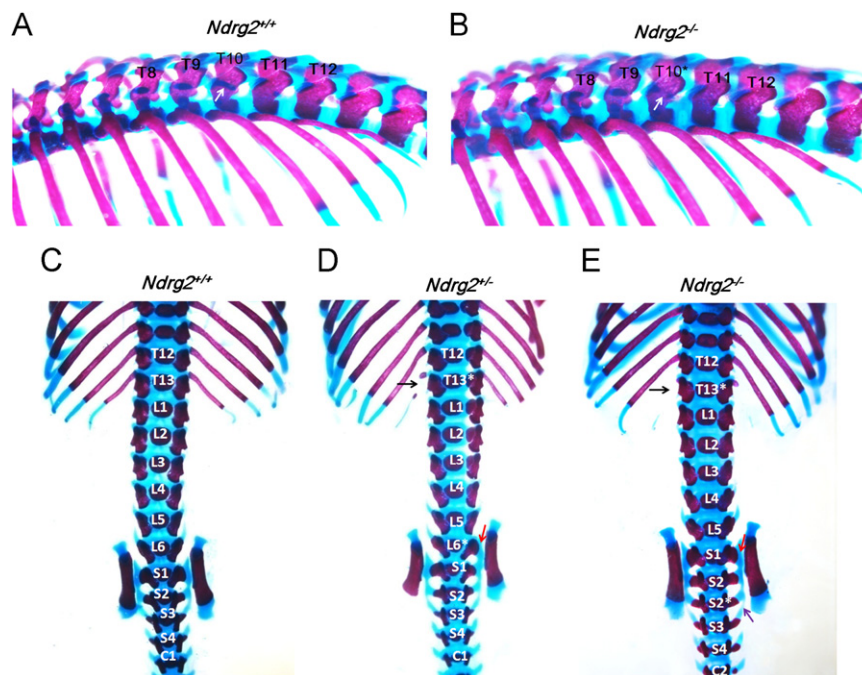


Fig. 3. Axial skeletal phenotypes in *Ndrgr2*-deficient mice. (A–B) Lateral view of the lower thoracic region. (C–E) Dorsal view of the posterior thoracic region to anterior caudal region. (A) The transitional vertebra is T10 in wild-type mice. The morphology of the costal facet in T10 (white arrow) is distinct from T11. (B) In *Ndrgr2* null mice, the T10 costal facet (white arrow) is similar to the T11 costal facet, indicating that the transitional vertebra shifts from T10 to T9. (C) Wild-type mice have 13 thoracic vertebrae and 6 lumbar vertebrae. (D) In *Ndrgr2*[±], the left rib on T13 is not fully developed (black arrow), denoting that T13 is partially transformed to L1. The 6th lumbar vertebra is fused with the transverse processes in the right side to form a sacral vertebra (red arrow), indicating a partial transformation to S1. (E) Much more severe vertebral defects are observed in *Ndrgr2*^{-/-}. The ribs on T13 disappeared (black arrow), and the L6 vertebrae are transformed to S1 (red arrow). In addition, the S4 transverse processes fuse to the S3 transverse processes (purple arrow), suggesting the transformation of S4 into S3. Asterisks indicate transformed vertebrae. All the samples are taken from newborn mice.

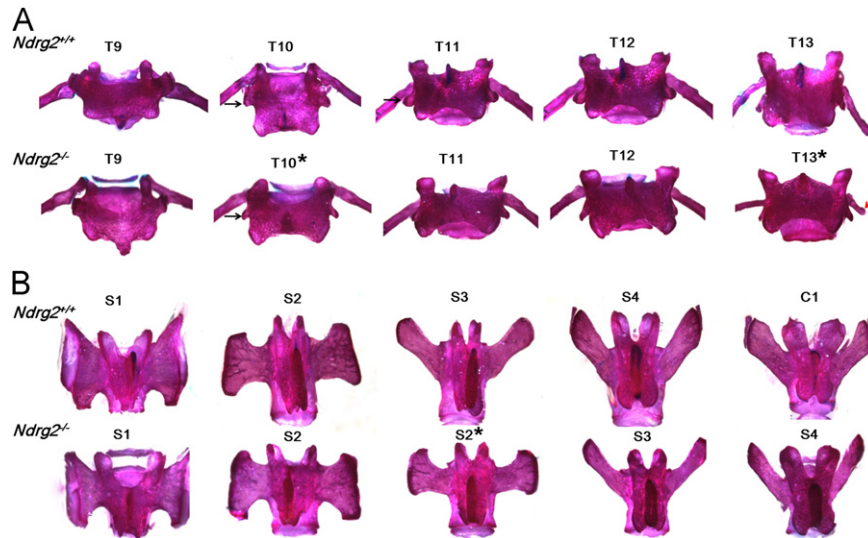


Fig. 4. Vertebral defects in *Ndr2* null mice. Dorsal view of individual thoracic (A) and sacral vertebrae (B) from 1-month-old wild-type littermate mice (upper row) and *Ndr2* null mice (lower row). (A) The overall shape of T10 in *Ndr2*^{-/-} is more similar to T11 than T10 in *Ndr2*^{+/+}. Black arrows point to costal facets. The red arrow indicates a rudimentary rib on T13. (B) The transverse processes of the S2* mutant (bottom arrow) have an intermediate shape. Asterisks indicate transformed vertebrae.

Table 1
Vertebral phenotypes in *Ndr2* mutants.

Genotype phenotype	WT n=44	<i>Ndr2</i> [±] n=17	<i>Ndr2</i> ^{-/-} n=15	<i>Col1a1-Cre; Ndr2</i> ^{cl/c} n=16	<i>Col2a1-Cre; Ndr2</i> ^{cl/c} n=15	<i>Col1a1-Ndr2</i> n=3 founders	<i>Col2a1-Ndr2</i> n=3 founders
Defect in C1	0/44 (0%)	0/17 (0%)	0/15 (0%)	0/16 (0%)	0/15 (0%)	1/3	0/3
T13 to L1	1/44 (2.3%)	7/17 (41%)	12/15 (80%)	7/16 (44%)	5/15 (33%)	0/3	0/3
L1 to T13	0/44 (0%)	0/17 (0%)	0/15 (0%)	0/16 (0%)	0/15 (0%)	2/3	3/3
L6 to S1	0/44 (0%)	14/17 (82%)	14/15 (93%)	14/16 (88%)	8/15 (53%)	0/3	0/3
S4 to S3	0/44 (0%)	12/17 (71%)	14/15 (93%)	11/16 (69%)	6/15 (40%)	3/3	3/3
Transitional vertebra							
T10	44 (100%)	11 (65%)	4 (27%)	12 (75%)	11 (73%)	1/3	3/3
T9	0 (0%)	6 (35%)	11 (73%)	4 (25%)	4 (27%)	2/3	0/3

thoracic vertebrae, 6 lumbar vertebrae, 4 sacral vertebrae and a variable number of caudal vertebrae (Green, 1941; O'Higgins and Johnson, 1993). In the *Ndr2*^{-/-} mice, the number of precaudal vertebrae was the same as in the wild type, while the organization of the vertebrae was altered. The transitional vertebra in the wild-type mice is at the level of the tenth thoracic vertebra (T10), which is known as the most anterior vertebra to show a lumbar rather than a thoracic articulation between the pre- and post-zygapophyses (Hostikka et al., 2009; Pollock et al., 1992), whereas the transition in *Ndr2*^{-/-} mice occurred at the ninth thoracic vertebra (T9). The T10 in the *Ndr2*^{-/-} mice was partially similar to the morphology of T11 in the wild-type mice (Fig. 3A and B, Fig. 4A). The ribs on the thirteenth thoracic vertebra (T13) were shortened or completely lost in the *Ndr2*^{-/-} mice, indicating a posterior transformation of the thirteenth thoracic vertebra (T13) into the first lumbar vertebra (L1) (black arrows in Fig. 3D and E). Meanwhile, the caudal lumbar vertebra (L6) underwent a similar transformation into the sacral vertebra (S1) in the *Ndr2*^{-/-} mutant (red arrows in Fig. 3D and E). In addition, the mutant S4 transverse processes fuse to the S3 transverse processes (purple arrow in Fig. 3E), and the mutant S3 processes (S2* in Fig. 4B) exhibited intermediate morphology between normal S2 and S3 processes. We noticed that the anterior and posterior homeotic transformations were detected in thoracic/lumbar and lumbar/sacral transitional regions which were vulnerable and preferentially affected in *Hox* mutants (Alexander et al., 2009). Furthermore, the *Ndr2*[±] mice had a milder phenotype with a lower penetrance than the *Ndr2*^{-/-} mice (Fig. 3D and E, Table 1). Taken

together, these vertebral transformations indicate that *Ndr2* modulates the vertebral specification in transitional regions in a dose-dependent manner.

Inactivation of Ndr2 does not perturb the clock signaling in PSM

The Wnt, Fgf, RA and Notch signaling pathways are early regulators of somitogenesis within the paraxial mesoderm (Alexander et al., 2009; Aulehla et al., 2003; Dubrulle et al., 2001; Ikeya and Takada, 2001; Kessel and Gruss, 1991; Partanen et al., 1998). As *Ndr2* was expressed in the PSM during somitogenesis (Fig. 1A), *Ndr2* possibly regulates vertebral identity in the PSM. To test this hypothesis, we examined the expression of several key components of these signaling pathways in *Ndr2*^{-/-} embryos. No change in the expression of *Fgf8* or *Notch1* was detected in the PSM at E10.5 (Fig. 5A, B, G and H). The expression of *Hey1* and *Spry2*, the readouts of Notch and Fgf signaling activity, respectively, was also intact in the PSM of *Ndr2*^{-/-} embryos (Fig. 5E, F, I and J). In addition, the expression of *Raldh2* (a RA marker) and *Dll1* (a receptor for *Notch1*) was also unchanged (Fig. 5C, D, K and L).

It has been reported that *Ndr2* attenuates Wnt/ β -catenin signaling in human colon cancer cell lines and B16F10 mouse melanoma cells (Yao et al., 2008). However, the expression of both *Wnt3a* and *Lef1* was not changed in *Ndr2*^{-/-} embryos (Fig. 5M, N, O and P). In our experiments, forced *Ndr2* overexpression did not alter Wnt/ β -catenin signaling in C3H10T1/2 or ATDC5 cells (data not shown). Furthermore, the *Ndr2*^{-/-} mice

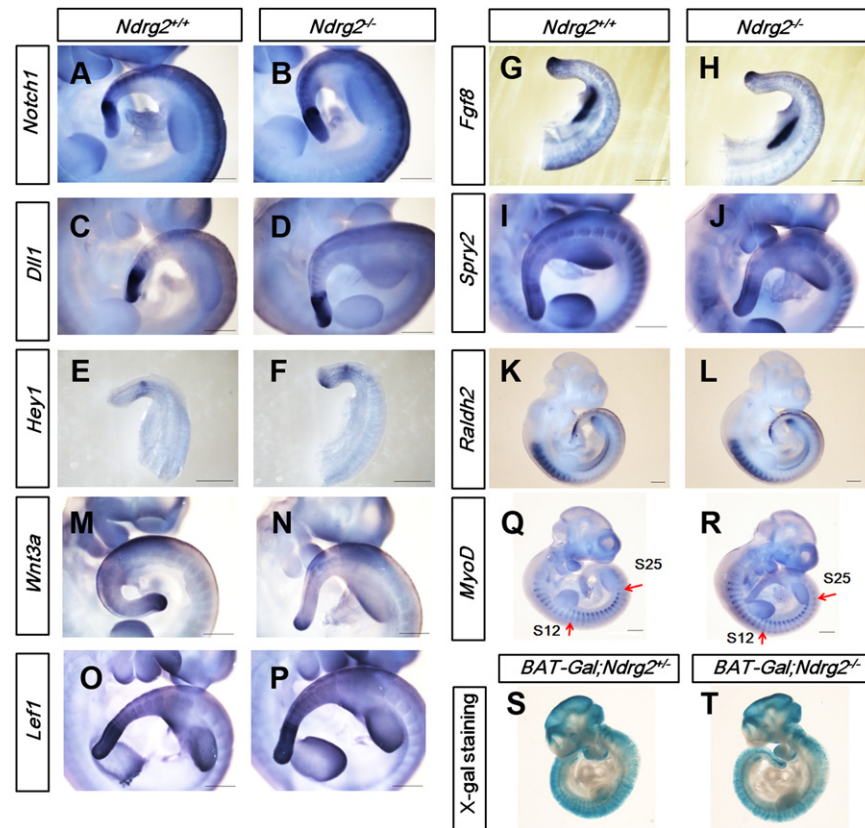


Fig. 5. Inactivation of *Ndr2* does not perturb major cyclic signaling in the PSM. (A–P) The Notch, Fgf, RA and Wnt signaling pathways are examined in embryos by whole mount in situ hybridization using various markers: *Notch1*, *Dll1* and *Hey1* for Notch signaling (A–F); *Fgf8* and *Spry2* for Fgf signaling (G–J); *Raldh2* for RA signaling (K, L); *Wnt3a* and *Lef1* for Wnt signaling (M–P). (Q, R) The number of somites visualized by *MyoD* is not altered in *Ndr2*-deficient embryos. Somite 12 and somite 25 are referenced as landmarks. All samples are at E10.5, and the experiments were repeated at least 2 times. (S, T) X-gal staining of *BatGal*; *Ndr2*[±] and *BatGal*; *Ndr2*^{-/-} embryos at E10.5. No significant difference is detected ($n=8$). Scale bar: 500 μ m.

were crossed with *BatGal* reporter mice to assess the *in vivo* Wnt/ β -catenin signaling activity. X-gal staining of the *Ndr2*^{-/-}; *BatGal* embryos at E10.5 was similar to that of *Ndr2*[±]; *BatGal* embryos (Fig. 5S and T), indicating that the Wnt/ β -catenin signaling activity was not affected in the *Ndr2*^{-/-} embryos. Additionally, the total number of segmented somites in the *Ndr2* null mutant, as marked by *MyoD* expression, was the same as in that the wild type (Fig. 5Q and R). These data suggest that the inactivation of *Ndr2* does not perturb the major oscillating signaling in the PSM or the overt somitogenesis at early stages.

Conditional inactivation or overexpression of *Ndr2* in differentiating somites produces vertebral transformations

As the inactivation of *Ndr2* did not perturb the expression of major oscillating genes, we speculated that *Ndr2* might regulate the somitic specification in differentiating somites rather than in the PSM. To validate this hypothesis, we generated conditional knockout mice in which *Ndr2* was specifically deleted through the *Col2a1-Cre* or *Col1a1-Cre* mice, which have Cre activity in chondrocytes or osteoblasts respectively (Liu et al., 2004; Ovchinnikov et al., 2000; Zha et al., 2008). Surprisingly, the *Col1a1-Cre*; *Ndr2*^{cl/c} and *Col2a1-Cre*; *Ndr2*^{cl/c} mice recapitulated all the vertebral defects observed in the *Ndr2* deficient mice with a lower penetrance (Fig. 6D and E, Table 1), including the anterior shift of the transitional vertebra from T10 to T9 and the homeotic transformations of T13–L1, L6–S1, and S3–S2.

Conversely, when *Ndr2* was overexpressed in the osteochondrogenitor cells driven by the *Col1a1* promoter (3.6 kb) or the *Col2a1* promoter (Liu et al., 2004; Ovchinnikov et al., 2000; Zha

et al., 2008), vertebral homeotic transformations in thoracic/lumbar and lumbar/sacral transitional regions in these transgenic mice were also detected (Fig. 6B and C, Table 1). In the *Col1a1-Ndr2* transgenic mice, C2 split into two parts in the dorsal region (red arrow in Fig. 6B, Table 1). In two of the three *Col1a1-Ndr2* transgenic founders, the transitional vertebra occurred at T9 instead of T10, as in the wild type (white arrow in Fig. 6B, Table 1). Furthermore, there were rudimentary ribs on the first lumbar vertebra (L1) in the *Col1a1-Ndr2* transgenic mice, indicating that L1 had a tendency towards anterior transformation into a thoracic vertebra (T13) (red arrows in Fig. 6B', Table 1). This transformation could be considered as the opposite of that observed at this location in the *Ndr2*-deficient mice. In addition, the *Col1a1-Ndr2* transgenic mice displayed a homeotic transformation of S3 into S2 (purple arrow in Fig. 6B) similar to that of *Ndr2*^{-/-}. Meanwhile, the *Col2a1-Ndr2* transgenic mice exhibited similar defects as the *Col1a1-Ndr2* mice except that the transitional vertebra was still T10 (arrows in Fig. 6C and C', Table 1). From the *Ndr2* loss-of-function and gain-of-function phenotypes in differentiating somites, it is reasonable to speculate that *Ndr2* is precisely controlled to regulate vertebral morphogenesis in the differentiating somites rather than in the PSM.

Expression levels of *Hox* genes in somites are differentially altered in *Ndr2* null embryos

Hox gene clusters play pivotal roles in regulating the patterning of somites, and their expression is considered to be a combinatorial code for somitic identity (Alexander et al., 2009;

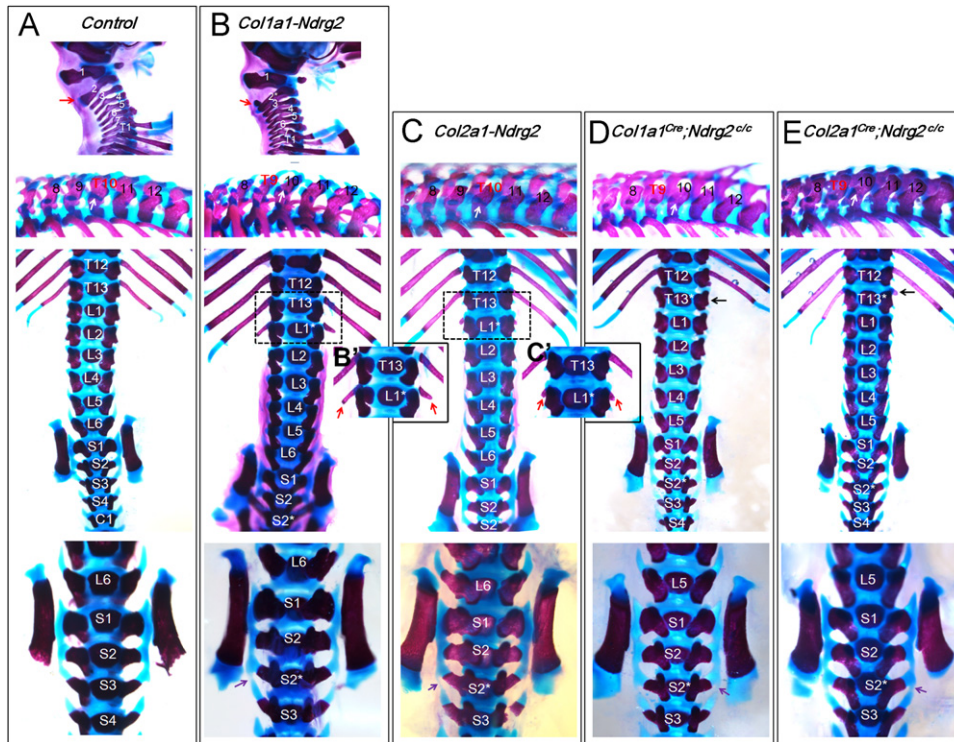


Fig. 6. Axial skeletal phenotypes in *Ndr2* transgenic and *Ndr2* conditional knockout mice. Side view of the cervical region (upper panel in A, B), lateral view of the lower thoracic region (middle panel in A, B; upper panel in C–E), dorsal view of the posterior thoracic region to anterior caudal region (middle panel), and dorsal view of the sacral region (bottom panel) for the wild-type (A), *Col1a1-Ndr2* (B), *Col2a1-Ndr2* (C), *Col1a1-Cre; Ndr2^{cl/c}* (D) and *Col2a1-Cre; Ndr2^{cl/c}* (E) mice. Vertebral identities are indicated in panels, with the transitional vertebra labeled in red. (A–C) In the *Col1a1-Ndr2* transgenic mice (B), C2 is split into two parts in the dorsal region (red arrow in B), the spinous processes on T9 and T10 are linked together (arrowhead) and the costal facet of T10 (white arrow in B) is similar to that of T11, indicating the transitional vertebra shifts from T10 to T9. In the *Col2a1-Ndr2* transgenic mice (C), the transitional vertebra is still T10. In both the *Col1a1-Ndr2* and *Col2a1-Ndr2* transgenic mice, there are rudimentary ribs on both sides of L1 (red arrows in B' and C'), and the S4 (S3*) transverse processes fuse to S3 transverse processes (purple arrows in B, C). (B', C') High-power view of the rectangular area in B and C. (D, E) *Col1a1-Cre; Ndr2^{cl/c}* and *Col2a1-Cre; Ndr2^{cl/c}* mice can recapitulate all the homeotic transformations observed in *Ndr2^{-/-}* mice. The white arrows, black arrows and purple arrows indicate the T10 costal facets and rudimentary ribs on the L1 and S4 (S3*) transverse processes, respectively. Asterisks indicate transformed vertebrae. All the *Ndr2* mutant mice were compared with wild-type littermates. For illustrative purposes, only the control for *Col1a1-Ndr2* is shown. The penetrances of these phenotypes are listed in Table 1.

Kessel and Gruss, 1991; Kmita and Duboule, 2003; Mallo et al., 2010; Wellik, 2007). To explore the mechanisms underlying the homeotic transformations in *Ndr2^{-/-}* mice, we examined the expression patterns of *Hoxa9-11*, *Hoxb9*, *Hoxc8-11*, and *Hoxd9-13* (Fig. 7 and Supplemental Fig. S1), which confer identity to the vertebrae from the middle thoracic region to caudal region (Alexander et al., 2009; Le Mouellic et al., 1992; Mallo et al., 2010; McIntyre et al., 2007; van den Akker et al., 2001; Wellik, 2007; Wellik and Capecchi, 2003). The examinations were conducted at E10.5, when the somite sclerotome from cervical to sacral level are beginning to undergo osteochondrogenic differentiation (Ovchinnikov et al., 2000). The overall expression level of *Hoxc8* and *Hoxc9* in somites was increased in *Ndr2^{-/-}* embryos with respect to the wild-type embryos (Fig. 7A–D). Conversely, the expression of *Hoxc10* and *Hoxc11* in somites at the prospective sacral level was impaired in the *Ndr2^{-/-}* embryos (red asterisks in Fig. 7E–H). The change of the amount of *Hoxc8-11* gene transcripts was validated by quantitative RT-PCR (Fig. 7I–L). The expression of the other *Hox* genes listed was unchanged in the null mutant (Supplemental Fig. S1). Furthermore, we examined the expression of *Hoxc8-11* and *Hoxa9-11* genes in *Col1a1-Ndr2* transgenic embryos (Supplemental Fig. S2). Slight but significant changes in the expression levels of *Hoxa9-10* and *Hoxc8-10* genes were detected. The alterations in *Hox* gene expression indicates that *Ndr2* regulates vertebral specification partially through regulating *Hox* genes expression.

According to previous reports, axial homeotic transformations are usually correlated with alterations in the expression boundaries

of the *Hox* genes (Ikeya and Takada, 2001; Kessel and Gruss, 1991; Partanen et al., 1998). Interestingly, the amount of transcripts rather than the expression boundaries of the *Hox* genes examined were altered in the *Ndr2^{-/-}* embryos compared to their wild-type littermates (Fig. 7 and Supplemental Fig. S1). These results are consistent with the notion that the expression boundaries of the *Hox* genes are mainly determined prior to somite segmentation (Alexander et al., 2009; Forlani et al., 2003; Imura and Pourquie, 2006).

Bmp signaling activity is elevated in the differentiating somites of *Ndr2^{-/-}* embryos

Numerous mutations of the *Bmp* signaling pathway also affect the axial AP patterning (Ikeya et al., 2006; Katagiri et al., 1998; McMahon et al., 1998; McPherron et al., 1999; Oh and Li, 1997). To investigate whether *Bmp* signaling was involved in the regulation of vertebral identity by *Ndr2*, we examined *Bmp4* expression as well as *Bmp*/*Smad* signaling activity in the *Ndr2^{-/-}* embryos at E10.5 and E11.5. We found that the expression of *Bmp4* in differentiating somites from thoracic to sacral level was grossly increased in *Ndr2^{-/-}* embryos compared to their control littermates, whereas *Bmp4* expression in limb buds was not obviously changed (Fig. 8A–B'). The *En-1* expression level was decreased in the corresponding somites in *Ndr2^{-/-}* embryos (Fig. 8C–D'). In fact, a similar alteration of *En-1* expression is detected in *Noggin^{-/-}* embryos, which are *Bmp* gain-of-function mutants (McMahon et al., 1998; Pizette et al., 2001). Moreover, *En-1* null

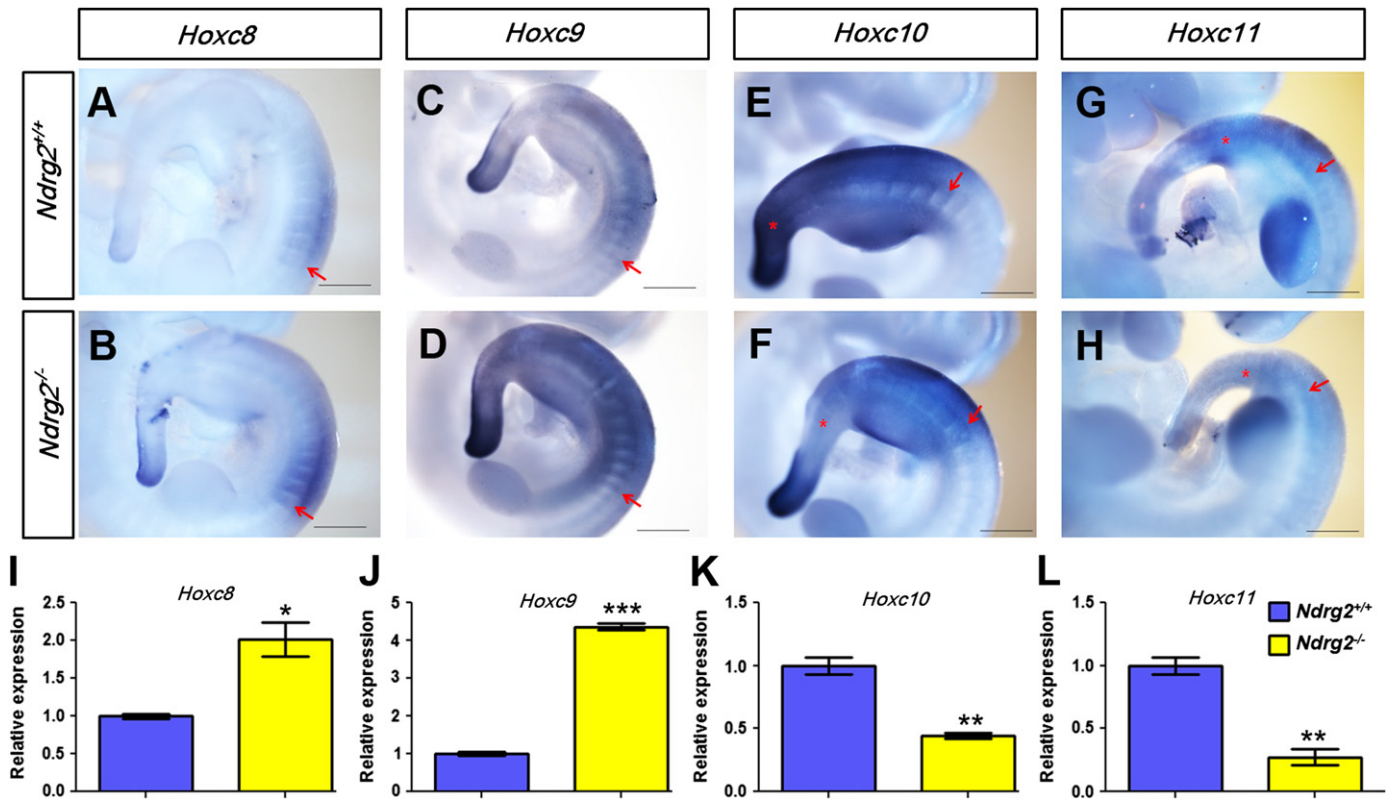


Fig. 7. Expression pattern of *Hox* genes in *Ndr2*-deficient embryos. The expression of *Hoxc8-11* is examined in wild-type and *Ndr2*^{-/-} embryos. (A–D) The expression levels of *Hoxc8* ($n=3$, A, B) and *Hoxc9* ($n=3$, C, D) are increased in the *Ndr2*^{-/-} embryos compared with littermate controls. (E–H) *Hoxc10* ($n=2$, E, F) and *Hoxc11* ($n=2$, G, H) expression levels are decreased in the prospective sacral somites (red asterisks) in *Ndr2*^{-/-} embryos compared with the littermate controls. Note that the anterior boundaries of *Hox* gene expression, which are marked by red arrows, are not significantly affected in *Ndr2*^{-/-} embryos. All the embryos are isolated at E10.5. Scale bar: 500 μ m. (I–L) The alterations of *Hoxc8-11* expression are validated by qRT-PCR. Total RNA is extracted from somites posterior to the 12th somite at E10.5. *Ndr2*^{-/-} embryos are compared with littermate controls ($n=4$). Values are represented as the means \pm SEM, and the relative mRNA expression is normalized to the β -actin gene expression level. * $p=0.0114$, *** $p < 0.0001$, ** $p < 0.0015$.

mice also exhibit vertebral transformation of T13–L1 (Wurst et al., 1994). The alterations of *Bmp4* and *En-1* expression were further validated by quantitative-PCR using RNA extracted from S12 to S25 of embryos at E10.5 (Fig. 8E and F). In addition to *Bmp4*, we also examined the expression of other *Bmp* ligands in *Ndr2* null embryos, such as *Bmp2*, *Bmp7* and *Gdf11*, which were expressed during axial skeleton development (Reshef et al., 1998). However, no significant alteration was observed for their expression levels (data not shown).

In the differentiating somites, IHC showed that p-Smad1/5/8 expression, an indicator of *Bmp*/*Smad* signaling activity, was elevated in the somitic mesoderm of *Ndr2*^{-/-} embryos compared to the wild-type embryos at E10.5 (Fig. 8G and H). The increase in p-Smad1/5/8 expression was further validated by western blotting of proteins isolated from S12 to S25 of E11.5 embryos (Fig. 8I and J). In addition, the in vitro overexpression of *Ndr2* downregulated *Bmp4* mRNA and p-Smad1/5/8 expression in murine ATDC5 cells, which also suggested a negative effect of *Ndr2* on *Bmp*/*Smad* signaling (Supplemental Fig. S3).

Discussion

In this paper, we investigated the function of *Ndr2* in modulating vertebral specification using *Ndr2* loss-of-function and gain-of-function mutants. Our results demonstrate that *Ndr2* is a novel regulator of vertebral specification, especially for the vertebrae in thoracic/lumbar and lumbar/sacral transitional regions. It may exert the effect through modulating *Bmp*/*Smad*

signaling and *Hox* gene expression in a dose-dependent manner. Nevertheless, *Ndr2* regulates vertebral identity and morphology in differentiating somites rather than in the PSM, which is distinct from the other regulators previously reported.

Ndr2 regulates vertebral patterning and morphogenesis in differentiating somites

Ndr2 was expressed early in the PSM and was dynamically expressed in differentiating somites. *Ndr2*-deficient mice exhibited vertebral defects in thoracic/lumbar and lumbar/sacral transitional regions: the transitional vertebra shifts from T10 to T9, and there are homeotic transformations of T13–L1, L6–S1 and S3–S2. Despite the several vertebral transformations at transitional regions, the total number of precaudal vertebrae in *Ndr2*^{-/-} was the same as that in the control. As the inactivation of *Ndr2* does not perturb the expression of major oscillating genes in the PSM, we speculate that *Ndr2* does not regulate somite generation in the PSM.

To further clarify the functional timing of *Ndr2*, we conditionally depleted *Ndr2* in osteochondrogenic cells using *Col1a1-Cre* and *Col2a1-Cre* transgenic mice, which have *Cre* activity in differentiating somites but not PSM. Both the *Col1a1-Cre; Ndr2*^{cl/c} and *Col2a1-Cre; Ndr2*^{cl/c} conditional knockout mice could fully recapitulate the defects observed in *Ndr2*^{-/-}, but with a lower penetrance. In contrast, the *Ndr2*-overexpressing *Col1a1-Ndr2* and *Col2a1-Ndr2* transgenic mice also exhibited vertebral homeotic transformations that were distinct from those in the *Ndr2*-deficient mice. These results indicate that the critical function of *Ndr2* occurs at the osteochondrogenic differentiation stage.

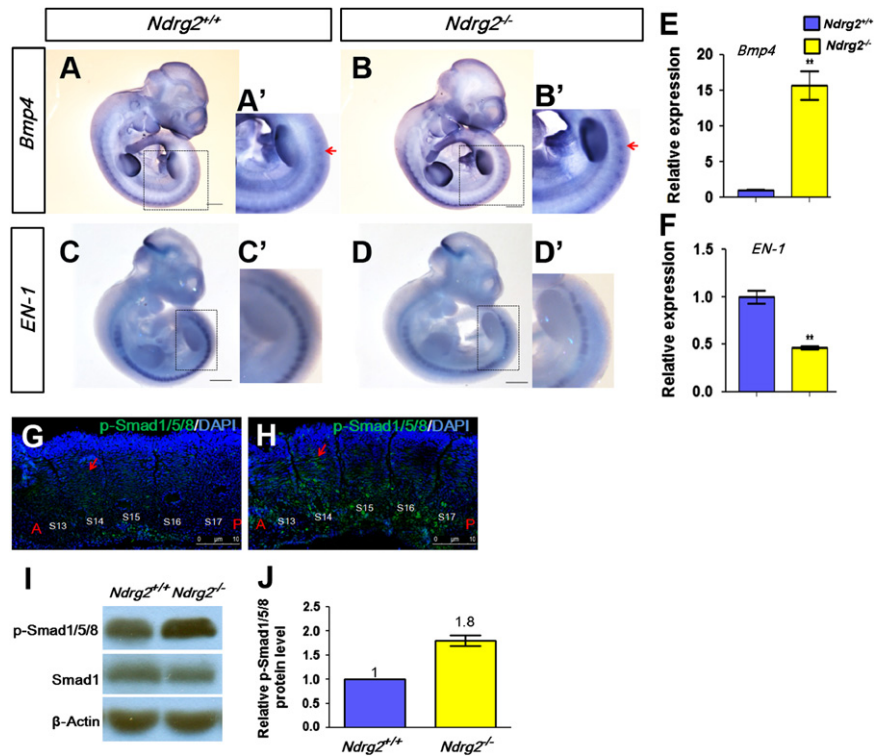


Fig. 8. *NdrG2* inhibits Bmp/Smad signaling in differentiating somites. (A–D) Expression levels of *Bmp4* and *EN-1* are examined in *NdrG2*^{+/+} (A, C) and *NdrG2*^{-/-} embryos (B, D) at E10.5. *Bmp4* expression is increased ($n=3$, A, B) whereas *EN-1* expression is decreased in somites ($n=3$, C, D). (A'–D') High-power view of the signal at the forelimb levels in (A–D), respectively. (E, F) qRT-PCR analysis confirms the changes in *Bmp4* and *EN-1* mRNA levels in *NdrG2*^{-/-} embryos compared with littermate wild-type controls ($n=4$). Total RNA was extracted from S12 to S15 (somites between forelimb and hindlimb) at E10.5. *NdrG2*^{-/-} embryos are compared with littermate controls ($n=4$). Values are represented as the means \pm SEM, and the relative mRNA expression is normalized to the β -actin gene expression level. ** $p < 0.0024$. (G, H) Immunostaining for p-Smad1/5/8 in sagittal sections of S13 to S17 from *NdrG2*^{+/+} (G) and *NdrG2*^{-/-} (H) embryos at E10.5. P-Smad1/5/8 is mainly detected in the somitic mesoderm (red arrow in G) of differentiating somites in *NdrG2*^{+/+}, whereas its expression is elevated and expanded in *NdrG2*^{-/-} somites (red arrow in H). This experiment was repeated independently at least 3 times, with similar results. (I) The p-Smad1/5/8 protein level is increased in *NdrG2*^{-/-} somites compared to wild-type somites according to western blot analysis. Protein was extracted from S12 to S25 cells at E11.5. β -actin and Smad1 are assayed as controls. This experiment was repeated independently twice. A, anterior; P, posterior; S, somite. Scale bar: 10 μ m (J) Quantification of relative p-Smad1/5/8 protein level in (I).

According to previous studies, the global patterning of somites occurs prior to somite formation (Alexander et al., 2009; Carapuco et al., 2005; Juan and Ruddle, 2003; Kiény et al., 1972; Nowicki and Burke, 2000). Our results suggest that vertebral identity remains plastic after somite segmentation. The vertebrae will fully acquire their identity under the guide of regulators in the differentiating somites such as *NdrG2*.

The effect of *NdrG2* on vertebral specification seems to be limited in thoracic/lumbar and lumbar/sacral transitional regions. A potential redundancy effect from another member of the *NdrG* family should be considered. The other *NdrG* family members (*NdrG1* and *NdrG3*) are also expressed in the somites and tail bud during axial skeletal development (our unpublished data) (Okuda and Kondoh, 1999). However, defects in the axial skeleton of *NdrG1*- and *NdrG4*-deficient mice have not been reported (Okuda et al., 2004; Taketomi et al., 2007; Yamamoto et al., 2011). It is possible that double or triple knockout of the *NdrG* genes would produce a much broader effect on vertebral specification. In fact, *Col1a1-NdrG2* transgenic mice have already extended their effect on the second cervical vertebrae.

NdrG2 modulates vertebral identity partially through the *Hox* genes

The vertebral homeotic transformations in *NdrG2*-deficient mice were correlated with alterations in *Hoxc8-11* gene expression levels. Based on the phenotypes of *Hox* gene loss-of-function mutants, the *Hox8-11* paralogous group is thought to confer the identity of the vertebrae from the mid-thoracic to the sacral region (Alexander et al., 2009; Le Mouellic et al., 1992; Mallo

et al., 2010; McIntyre et al., 2007; van den Akker et al., 2001; Wellik, 2007; Wellik and Capecchi, 2003). In *NdrG2*^{-/-} embryos, both the *Hoxc8* and *Hoxc9* expression levels in the somites were increased, whereas the *Hoxc10* and *Hoxc11* expression levels were decreased compared to those of the controls. Loss of *Hoxc8* or *Hoxc9* in somites leads to several homeotic transformations of L1 into T13 and the shift of transitional vertebra from T10 to T13 (Le Mouellic et al., 1992; Suemori et al., 1995), which are effects opposite to those of the *NdrG2* null mutation. Conversely, *Hoxc10*-deficient mice display homeotic transformations similar to those observed in the *NdrG2*-deficient mice (Hostikka et al., 2009). In addition, the changes in *Hoxc8-10* genes expression levels were also detected in *Col1a1-NdrG2* transgenic embryos. Of note, alterations in the amount of *Hoxc8-11* transcripts, but not their expression boundaries, were detected in differentiating somites in *NdrG2*^{-/-} mice. The impact of quantitative variations of *Hox* gene expression on vertebral identity was not previously reported. Therefore, we speculate that the combinatory alterations in *Hox* genes expression levels could partially, even if not solely, account for the vertebral defects in *NdrG2*-deficient mice.

NdrG2 inhibits Bmp signaling in the mesoderm of differentiating somites

Bmp signaling plays an important role during mouse somite development and osteochondrogenic differentiation (Ikeya et al., 2006; Katagiri et al., 1998; McMahon et al., 1998; McPherron et al., 1999; Miura et al., 2006; Oh and Li, 1997). In *NdrG2*-deficient embryos at E10.5, both the *Bmp4* mRNA

expression and p-Smad1/5/8 protein levels were elevated, indicating an increase in Bmp/Smad signaling activity. Conversely, forced expression of *Ndr2* in ATDC5 cells results in reduced *Bmp4* mRNA expression and decreased Bmp/Smad signaling activity. It seems that *Ndr2* selectively inhibit *Bmp4* expression, but not the other Bmp ligands such as *Bmp2*, *Bmp7* and *Gdf11*, in differentiating somites (data not shown). In fact, in an analysis of the *Noggin* mutation, a previous report showed that the inhibition of Bmp signaling is essential for the chondrogenic differentiation of the somitic mesoderm (McMahon et al., 1998).

Taken together, our results suggest that *Ndr2* regulate vertebral specification in differentiating somites, partially through the *Hox* genes and Bmp signaling. However, the molecular mechanisms of this regulation remain to be addressed in the future.

Acknowledgments

We thank Prof. Baojie Li for providing us with the *Actin-Cre* mice. We thank Prof. Xiao Yang for providing us the *Col1a1* (3.6 kb)-*Cre* mice. This work was supported by the National Major Fundamental Research 973 program of China under grant (2007CB947301 and 2012CB966903) and grants from the National Natural Science Foundation of China (31171396, 81121001 and 31100624).

Appendix A. Supporting information

Supplementary data associated with this article can be found in the online version at <http://dx.doi.org/10.1016/j.ydbio.2012.07.001>.

References

- Alexander, T., et al., 2009. Hox genes and segmentation of the hindbrain and axial skeleton. *Annu. Rev. Cell Dev. Biol.* 25, 431–456.
- Aulehla, A., et al., 2003. Wnt3a plays a major role in the segmentation clock controlling somitogenesis. *Dev. Cell* 4, 395–406.
- Burke, A.C., et al., 1995. Hox genes and the evolution of vertebrate axial morphology. *Development* 121, 333–346.
- Cambray, N., Wilson, V., 2007. Two distinct sources for a population of maturing axial progenitors. *Development* 134, 2829–2840.
- Carapuco, M., et al., 2005. Hox genes specify vertebral types in the presomitic mesoderm. *Genes Dev.* 19, 2116–2121.
- Dequeant, M.L., Pourquie, O., 2008. Segmental patterning of the vertebrate embryonic axis. *Nat. Rev. Genet.* 9, 370–382.
- Dubrule, J., Pourquie, O., 2004. Coupling segmentation to axis formation. *Development* 131, 5783–5793.
- Dubrule, J., et al., 2001. FGF signaling controls somite boundary position and regulates segmentation clock control of spatiotemporal Hox gene activation. *Cell* 106, 219–232.
- Dupays, L., et al., 2009. Tbx2 misexpression impairs deployment of second heart field derived progenitor cells to the arterial pole of the embryonic heart. *Dev. Biol.* 333, 121–131.
- Foletta, V.C., et al., 2009. NDRG2, a novel regulator of myoblast proliferation, is regulated by anabolic and catabolic factors. *J. Physiol.* 587, 1619–1634.
- Forlani, S., et al., 2003. Acquisition of Hox codes during gastrulation and axial elongation in the mouse embryo. *Development* 130, 3807–3819.
- Green, E.L., 1941. Genetic and non-genetic factors which influence the type of the skeleton in an inbred strain of mice. *Genetics* 26, 192–222.
- Guo, X., et al., 2004. Wnt/beta-catenin signaling is sufficient and necessary for synovial joint formation. *Genes Dev.* 18, 2404–2417.
- Hirsinger, E., et al., 2000. Somite formation and patterning. *Int. Rev. Cytol.* 198, 1–65.
- Hostikka, S.L., et al., 2009. Axial and appendicular skeletal transformations, ligament alterations, and motor neuron loss in *Hox10* mutants. *Int. J. Biol. Sci.* 5, 397–410.
- Hu, X.L., et al., 2006. Expression analysis of the NDRG2 gene in mouse embryonic and adult tissues. *Cell Tissue Res.* 325, 67–76.
- Hwang, J., et al., 2011. Crystal structure of the human N-Myc downstream-regulated gene 2 protein provides insight into its role as a tumor suppressor. *J. Biol. Chem.* 286, 12450–12460.
- limura, T., Pourquie, O., 2006. Collinear activation of *Hoxb* genes during gastrulation is linked to mesoderm cell ingression. *Nature* 442, 568–571.
- limura, T., Pourquie, O., 2007. Hox genes in time and space during vertebrate body formation. *Dev. Growth Differ.* 49, 265–275.
- limura, T., et al., 2009. Establishment of Hox vertebral identities in the embryonic spine precursors. *Curr. Top Dev. Biol.* 88, 201–234.
- Ikeya, M., Takada, S., 2001. Wnt-3a is required for somite specification along the anteroposterior axis of the mouse embryo and for regulation of *cdx-1* expression. *Mech. Dev.* 103, 27–33.
- Ikeya, M., et al., 2006. Essential pro-Bmp roles of crossveinless 2 in mouse organogenesis. *Development* 133, 4463–4473.
- Juan, A.H., Ruddle, F.H., 2003. Enhancer timing of Hox gene expression: deletion of the endogenous *Hoxc8* early enhancer. *Development* 130, 4823–4834.
- Katagiri, T., et al., 1998. Skeletal abnormalities in doubly heterozygous *Bmp4* and *Bmp7* mice. *Dev. Genet.* 22, 340–348.
- Kessel, M., Gruss, P., 1991. Homeotic transformations of murine vertebrae and concomitant alteration of Hox codes induced by retinoic acid. *Cell* 67, 89–104.
- Kieny, M., et al., 1972. Early regionalization of somitic mesoderm as studied by the development of axial skeleton of the chick embryo. *Dev. Biol.* 28, 142–161.
- Kmita, M., Duboule, D., 2003. Organizing axes in time and space; 25 years of colinear tinkering. *Science* 301, 331–333.
- Krumlauf, R., 1994. Hox genes in vertebrate development. *Cell* 78, 191–201.
- Le Mouellic, H., et al., 1992. Homeosis in the mouse induced by a null mutation in the *Hox-3.1* gene. *Cell* 69, 251–264.
- Lee, Y.J., et al., 2010. Growth differentiation factor 11 signaling controls retinoic acid activity for axial vertebral development. *Dev. Biol.* 347, 195–203.
- Li, Y., et al., 2011. N-myc downstream-regulated gene 2, a novel estrogen-targeted gene, is involved in the regulation of Na⁺/K⁺-ATPase. *J. Biol. Chem.* 286, 32289–32299.
- Liu, F., et al., 2004. Expression and activity of osteoblast-targeted Cre recombinase transgenes in murine skeletal tissues. *Int. J. Dev. Biol.* 48, 645–653.
- Liu, W., et al., 2012. N-myc downstream regulated gene 1 modulates Wnt-beta-catenin signalling and pleiotropically suppresses metastasis. *EMBO Mol. Med.* 4, 93–108.
- Maconochie, M., et al., 1996. Paralogous Hox genes: function and regulation. *Annu. Rev. Genet.* 30, 529–556.
- Mallo, M., et al., 2010. Hox genes and regional patterning of the vertebrate body plan. *Dev. Biol.* 344, 7–15.
- McIntyre, D.C., et al., 2007. Hox patterning of the vertebrate rib cage. *Development* 134, 2981–2989.
- McMahon, J.A., et al., 1998. Noggin-mediated antagonism of BMP signaling is required for growth and patterning of the neural tube and somite. *Genes Dev.* 12, 1438–1452.
- McPherron, A.C., et al., 1999. Regulation of anterior/posterior patterning of the axial skeleton by growth/differentiation factor 11. *Nat. Genet.* 22, 260–264.
- Miura, S., et al., 2006. BMP signaling in the epiblast is required for proper recruitment of the prospective paraxial mesoderm and development of the somites. *Development* 133, 3767–3775.
- Nowicki, J.L., Burke, A.C., 2000. Hox genes and morphological identity: axial versus lateral patterning in the vertebrate mesoderm. *Development* 127, 4265–4275.
- O'Higgins, P., Johnson, D.R., 1993. The inheritance of vertebral shape in the mouse. II. A study using Fourier analysis to examine the inheritance of patterns of vertebral variation in the cervical and upper thoracic vertebral column. *J. Anat.* 182 (Pt 1), 65–73.
- Oh, S.P., Li, E., 1997. The signaling pathway mediated by the type IIB activin receptor controls axial patterning and lateral asymmetry in the mouse. *Genes Dev.* 11, 1812–1826.
- Oh, S.P., et al., 2002. Activin type IIA and IIB receptors mediate Gdf11 signaling in axial vertebral patterning. *Genes Dev.* 16, 2749–2754.
- Okuda, T., Kondoh, H., 1999. Identification of new genes *ndr2* and *ndr3* which are related to *Ndr1/RTP/Drg1* but show distinct tissue specificity and response to N-myc. *Biochem. Biophys. Res. Commun.* 266, 208–215.
- Okuda, T., et al., 2004. *Ndr1*-deficient mice exhibit a progressive demyelinating disorder of peripheral nerves. *Mol. Cell Biol.* 24, 3949–3956.
- Ovchinnikov, D.A., et al., 2000. *Col2a1*-directed expression of Cre recombinase in differentiating chondrocytes in transgenic mice. *Genesis* 26, 145–146.
- Partanen, J., et al., 1998. Opposite phenotypes of hypomorphic and Y766 phosphorylation site mutations reveal a function for *Fgf1* in anteroposterior patterning of mouse embryos. *Genes Dev.* 12, 2332–2344.
- Pizette, S., et al., 2001. BMP controls proximodistal outgrowth, via induction of the apical ectodermal ridge, and dorsoventral patterning in the vertebrate limb. *Development* 128, 4463–4474.
- Pollock, R.A., et al., 1992. Altering the boundaries of *Hox3.1* expression: evidence for antipodal gene regulation. *Cell* 71, 911–923.
- Pourquie, O., 2011. Vertebrate segmentation: from cyclic gene networks to scoliosis. *Cell* 145, 650–663.
- Reshef, R., et al., 1998. Regulation of dorsal somitic cell fates: BMPs and Noggin control the timing and pattern of myogenic regulator expression. *Genes Dev.* 12, 290–303.
- Suemori, H., et al., 1995. *Hoxc-9* mutant mice show anterior transformation of the vertebrae and malformation of the sternum and ribs. *Mech. Dev.* 51, 265–273.
- Takahashi, K., et al., 2005. *Ndr2* promotes neurite outgrowth of NGF-differentiated PC12 cells. *Neurosci. Lett.* 388, 157–162.
- Taketomi, Y., et al., 2007. Impaired mast cell maturation and degranulation and attenuated allergic responses in *Ndr1*-deficient mice. *J. Immunol.* 178, 7042–7053.

- Tschopp, P., Duboule, D., 2011. A genetic approach to the transcriptional regulation of Hox gene clusters. *Annu. Rev. Genet.* 45, 145–166.
- van den Akker, E., et al., 2001. Axial skeletal patterning in mice lacking all paralogous group 8 Hox genes. *Development* 128, 1911–1921.
- Wellik, D.M., 2007. Hox patterning of the vertebrate axial skeleton. *Dev. Dyn.* 236, 2454–2463.
- Wellik, D.M., 2009. Hox genes and vertebrate axial pattern. *Curr. Top. Dev. Biol.* 88, 257–278.
- Wellik, D.M., Capecchi, M.R., 2003. Hox10 and Hox11 genes are required to globally pattern the mammalian skeleton. *Science* 301, 363–367.
- Wurst, W., et al., 1994. Multiple developmental defects in *Engrailed-1* mutant mice: an early mid-hindbrain deletion and patterning defects in forelimbs and sternum. *Development* 120, 2065–2075.
- Yamamoto, H., et al., 2011. NDRG4 protein-deficient mice exhibit spatial learning deficits and vulnerabilities to cerebral ischemia. *J. Biol. Chem.* 286, 26158–26165.
- Yang, J., et al., 2010. NDRG2 in rat liver regeneration: role in proliferation and apoptosis. *Wound Repair Regen.* 18, 524–531.
- Yao, L., et al., 2008. NDRG2: a Myc-repressed gene involved in cancer and cell stress. *Acta Biochim. Biophys. Sin. (Shanghai)* 40, 625–635.
- Young, T., Deschamps, J., 2009. Hox, Cdx, and anteroposterior patterning in the mouse embryo. *Curr. Top. Dev. Biol.* 88, 235–255.
- Zha, L., et al., 2008. Collagen1alpha1 promoter drives the expression of Cre recombinase in osteoblasts of transgenic mice. *J. Genet. Genomics* 35, 525–530.
- Zhu, X., et al., 2012. Wls-mediated Wnts differentially regulate distal limb patterning and tissue morphogenesis. *Dev. Biol.*